Tuning the Thermal Isomerization of Phenylazoindole Photoswitches from Days to Nanoseconds

Nadja A. Simeth,[†,‡] Stefano Crespi,[§,‡] Maurizio Fagnoni[§] and Burkhard König[†,*]

[†] Institut für Organische Chemie, Universität Regensburg, Universitätsstraße 31, 93040 Regensburg, Germany.

[§] PhotoGreen Lab, Università di Pavia, Via Taramelli 12, 27100 Pavia, Italy.

ABSTRACT: The growing interest in light-driven molecular switches and optical oscillators led to the development of molecules that are able to interconvert from a stable to a metastable configuration upon photochemical triggering and to return to the thermodynamically stable form as soon as the light stimulus is removed. Controlling a wide range of back-isomerization lifetimes in the dark is a crucial goal for potential application of these compounds such as molecular machines. We herein present a novel class of easily synthesizable azo photoswitches based on the arylazoindole core. Most notably, minimal modifications of the core such as the methylation, dramatically change the *Z*-to-*E* thermal isomerization rate from days (Me in position 1) to the nanosecond range (Me in position 2). Moreover, fine tuning of the *Z*-to-*E* lifetimes can be achieved choosing a proper dimethylsulfoxide-water (or buffered water) solvent mixture. The photochemical and thermal mechanisms have been elucidated by a thorough computational and spectroscopic analysis. This allowed to detect three different pathways of thermal isomerization and to identify the hydrazone tautomer of the phenylazoindole as the major actor in the fast *Z*-*E* thermal isomerization of the NH-substituted switch in protic media.

INTRODUCTION

Photoswitches have evolved into handy tools to control molecular properties, such as magnetization, fluorescence or biological activity, or can be exploited as the centerpiece of molecular machines.[1] Thereby, light is applied as an external stimulant. It is easy to handle, unmatchable fast and precise in practical usage, and orthogonal to biological systems and most chemical transformations.[1–3] Within the many classes of photoswitches investigated, azo dyes have emerged as a popular example in the last decades including manifold applications, e.g. in polymers,[4,5] electronics,[6] material science,[7] protein probes and *in-vivo* photo-control of biomolecules,[8–11] or as light-controllable catalysts.[12] Among them, azobenzene (and its derivatives) is undoubtedly the most prominent scaffold investigated in both fundamental research and modern applications.[13] The planar azobenzene *E*-isomer can be efficiently converted into its meta-stable *Z*-isomer *via* UV irradiation, with a consequent change in the electronic as well as geometrical properties of the molecule.[14,15] The *Z*-isomer is the main component of the thus formed photostationary state (PSS) and can interconvert to the more stable *E*-isomer through visible light irradiation or through thermal relaxation.[15] Indeed, the ideal thermal lifetime of the meta-stable *Z*-isomer strongly depends on the application of interest. Highly thermal stable azoswitches are desired for applications as such as molecular storage or logic devices, respectively.[16] In contrast, fast relaxing azobenzenes are preferably employed, for instance, in real-time optical information-transmitting materials[17] or in *in-vivo* applications due to their temporally limited action.[18] Thus, a lot of effort has been put to modify the thermal lifetime of azobenzenes. Most of these transformations have been achieved through the introduction of different substituents onto the azobenzene core. Ortho-fluoro[19] or ortho-thiol substituents[20] have been used to stabilize the thermal lifetime of azobenzenes, whereas 4,4′ push-pull or azophenolic systems (or a combination of both) can lead to extremely fast-relaxing switches.[17,21] More recently, also heteroaromatic scaffolds were considered to broaden the range of azo dye properties, including their thermal lifetime. Notably, azopyrimidine,[21] azopyridines,[22,23] azopyrroles,[24] azoimidazole[25–29] and azopyrazoles,[30–32] or lately the bicyclic azoindazole scaffold,[33] were reported. They were used, for example, to control the assembly of supramolecular systems or as photo-controllable ligands being, depending on the scaffold and its substitution pattern, highly stable (for a pyrazole derivative, the thermal lifetime is reported to be up to 1000 days[32]) or fast-relaxing systems (40 ns, for an azopyrimidine[21]). However, a scaffold usually exhibits a certain lifetime and the tunability is mostly limited to few orders of magnitude, thus it belongs either to the thermally stable or to the fast back-isomerizing family.

Herein, we present phenylazoindoles as photochromic scaffolds with extremely tunable thermal lifetimes. Indoles are omnipresent in nature, substructures of drugs and various dyes. Though previously employed as antibacterial agents, food-dyes,[34] or metal complexing ligands,[35] arylazoindoles have not been considered as photochromic compounds so far. We investigated both minimal chemical variations of the scaffold (methylation in different positions) and solvent effects on the thermal lifetime of the compounds. We elucidated the mechanism of the isomeri-

zations and take advantage of it to tune the properties of the here presented photoswitches from days to nanoseconds. Thereby, we focus on providing a deep and general understanding of a new class of azo photoswitches to pave the way to further rational developments, using this novel core potentially for all kinds of applications.

RESULTS AND DISCUSSION

Synthesis. The phenylazoindoles **3a-c** were synthesized through azocoupling of diazonium salt **2** and the appropriate indoles **1a-c** (see Scheme 1 and Section 2 in the Supporting Information).

Scheme 1. Synthesis of 3a-c.

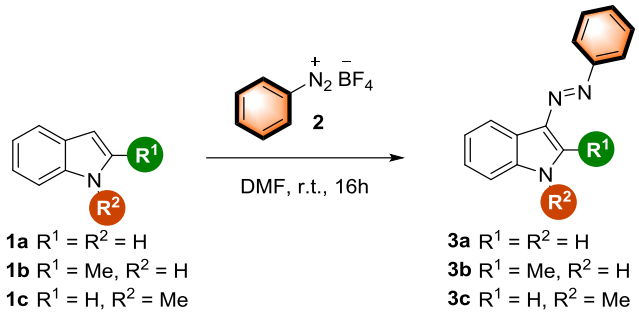

1a $R^1 = R^2 = H$
1b $R^1 = Me$, $R^2 = H$
1c $R^1 = H$, $R^2 = Me$

3a $R^1 = R^2 = H$
3b $R^1 = Me$, $R^2 = H$
3c $R^1 = H$, $R^2 = Me$

Spectroscopy. The absorption and isomerization properties of phenylazoindoles **3a-c** were investigated in various solvents, from non-polar (aromatic and non-aromatic) to polar aprotic and polar-protic ones. Most prominent is the broad absorption band between 359 and 380 nm. We could assign the aforementioned band to the $\pi\rightarrow\pi^*$ transition of the azo group (see Table S1; for the recorded UV/Vis spectra, see Section 3 in the Supporting) owing to the similarities with azobenzene and other azoheteroarenes, and TD-DFT simulations (see Section 5.3 in the Supporting).[15,33] By trend, methylation (**3b** and **3c**) induces a slight bathochromic shift of the band compared to **3a** (between 4 to 11 nm). The weaker $n\rightarrow\pi^*$ band is present between 400 to 500 nm as a tailing of the $\pi\rightarrow\pi^*$ transition. Due to the high variety of lifetimes (τ) of the *Z*-isomer encountered, we decided to study the different kinetics of thermal relaxation processes of ***Z*-3a-c** using three different experimental setups. In particular, for the slower kinetics, the *E*-to-*Z* isomerization was induced through irradiation with LEDs of 400 nm or 365 nm and the back isomerization from the PSS in the dark was recorded through an UV/Vis spectrometer (seconds to hours range, see for example Figure 1A) or multiplate UV/Vis reader (hours to days). The faster kinetics were studied via nanosecond laser flash photolysis with excitation provided by a Nd:YAG laser at 355 nm (full details and pictures of the various experimental setups are included in the Supporting Information, Section 1). Multiple isomerization cycles can be achieved by pulsed irradiation of a single wavelength (see for example Figure 1B, concerning the pulsed irradiation with 400 nm of **3a** in DMSO).

The results are summarized in Table 1 (see Table S2 for a wider number of entries, spectra and isomerization kinetics). Compounds ***Z*-3a** and ***Z*-3b** exhibited thermal isomerization lifetimes comparable with or far lower than the second range. Laser flash photolysis allowed us to describe the transient absorption signal belonging to the *Z*-form of **3a** and **3b**. In particular, in **3b** a broad absorption band appeared around 450 nm immediately after the laser shot, attributable to the $n\rightarrow\pi^*$ transition of its *Z*-isomer (Figure 1C). On the other hand, only the bleaching of the $\pi\rightarrow\pi^*$ of the *E*-isomer can be observed in **3a**. TD-DFT UV/Vis absorption simulations of the most stable Z- isomers of **3a,b** allowed us to conclude that the geometry of ***Z*-3b** is causing the $n\rightarrow\pi^*$ transition to be more symmetry-allowed than the one in ***Z*-3a** (cf. Section 5.3 in the Supporting Information).

Moving from apolar to polar-aprotic solvents in **3a** led to τ shifting from the millisecond to the second range (Entries 1-5, 12-13, Table 1). This trend becomes less discernible with ***Z*-3b**, which only in dioxane has a $\tau > 1$ s (entry 2, Table 1). In **3a,b** it seems that the increased speed of the thermal *Z*-to-*E* relaxation goes hand in hand with the proton-availability (compare entries 7 and 13 for ***Z*-3a**). A striking example is **3a** in mixtures of MeOH or DMSO with water. While the addition of water in methanol does not drastically modify the lifetime (cf. Table 1, entry 7, 9, 10 for ***Z*-3a**), the increased protic environment in aprotic DMSO lowers τ from seconds to microseconds (cf. Table 1, entry 13-15). This allowed tuning the lifetime only by changing the water-content in DMSO. Similar observations can be made for ***Z*-3b**. Here, 1:1 mixtures of water and MeOH or DMSO afford lifetimes of 41.4 μs or 32.1 μs, respectively. Moreover, in a mixture of acidic water and DMSO, the relaxation time decreases to 2.2 μs for ***Z*-3a** and even reaches the nano-second range (743 ns) for ***Z*-3b** (entry 16). A similar result was obtained for both **3a** and **3b** when DBU was used as additive (entry 17), suggesting a proton-transfer mechanism contributes to the speed of the thermal isomerization. Reaching the sub-microsecond scale is crucial for applications requiring real-time information transmission, and up to now, this goal was achieved in azobenzene cores only in one case by using phenolic push-pull systems.[21] The dependency on protic environment becomes more evident comparing the lifetimes of ***Z*-3a** in MeOH and MeOD, which show a significant kinetic isotope effect (entries 7 and 8 in Table 1). A KIE=5.5 indicates that a proton transfer is involved in the rate-determining step in this solvent. Increasing the concentration of **3a** in MeOH leads to faster isomerization kinetics (entry 11). In anhydrous toluene no concentration effect on τ was found, see Table S2. The presence of an intermolecular interaction in **3a** can be followed by NMR (see Section 4.3 in the Supporting Information). In contrast to the other experiments, ***Z*-3b** in methanol relaxes with a biexponential kinetic. This suggests, compared with the previous findings, that the presence of a protic environment modifies the mechanism of the dark reaction for ***Z*-3a** and ***Z*-3b**. Indeed, for the specific case of **3b** in MeOH, two mechanisms of thermal relaxation are in competition (cf. entry 7 for **3b**). A detailed kinetic analysis of the thermal isomerization reaction is present in Section 7 of the Supporting Information. In particular, both a dependency on concentration of the photoswitch and on water was found for the N-H containing photoswitch **3b**. The kinetic law that was derived is similar to the one obtained for the arylazoimidazoles, compounds that are supposed to

isomerize through an intermolecular proton transfer leading to the formation of a hydrazone intermediate (Chart 1).[17,26,32]

Chart 1. Formula of the *s*-trans Hydrazone Tautomer of 3a,b

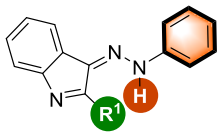

R^1 = H, Me

Table 1. *Z*-to-*E* Isomerization Lifetimes for 3a-c.

Entry	Solvents[a]	Lifetime τ		
		3a	3b	3c[c]
1	cyclohexane	42.5 ms[b]	116.8 ms[b]	1.1 h
2	dioxane	84.9 ms[b]	1.9 s[c]	17.6 h
3	mesitylene	12.3 ms[b]	3.3 ms[b]	1.13 d
4	benzene	78.5 ms[b]	167 ms[b]	6.0 min
5	toluene	47.5 ms[b]	60.2 ms[b]	17.1 min
6	aqueous toluene[d]		1.4 ms[b]	
7	MeOH	6.8 ms[b]	454 μs (51%), 78 μs (49%) [e]	2.4 h
8	MeOD	37.7 ms[b]		
9	MeOH water 9:1	14.8 ms[b]	41.9 μs[b]	
10	MeOH water 1:1	2.9 ms[b]	41.4 μs[b]	
11	MeOH[f]	4.7 ms[b]		
12	MeCN (dry)	4.3 s[c]	1.9 μs[b]	1.2 d
13	DMSO (dry)	6.5 s[c]	1.3 ms[b]	2.6 d
14	DMSO water 9:1	266 μs[b]	111.2 μs[b]	
15	DMSO water 1:1	187.9 μs[b]	32.1 μs[b]	
16	DMSO - buffered water (pH = 4)[f] 1:1	2.2 μs[b]	743 ns[b]	
17	DMSO water 1:1 + 25 μL DBU	31 ns	46 ns	

[a] The concentration was adjusted to 50 μM for all the measurements. [b] Determined *via* nanosecond laser flash photolysis. [c] Determined *via* UV/Vis spectroscopy. [d] Toluene saturated with water (15 μL of water were added to 2 mL of a 50 μM solution of **3b** in toluene. The emulsion thus formed was sonicated for 1h.) [e] The decay is biexponential. In parentheses is shown the contribution of the single lifetimes to the whole decay. [f] Concentration of **3a** = 75 μM [g] pH = 4.00 ± 0.02 (20 °C) (Citric acid = 0.056 M; NaOH = 0.11 M; HCl = 0.044 M)

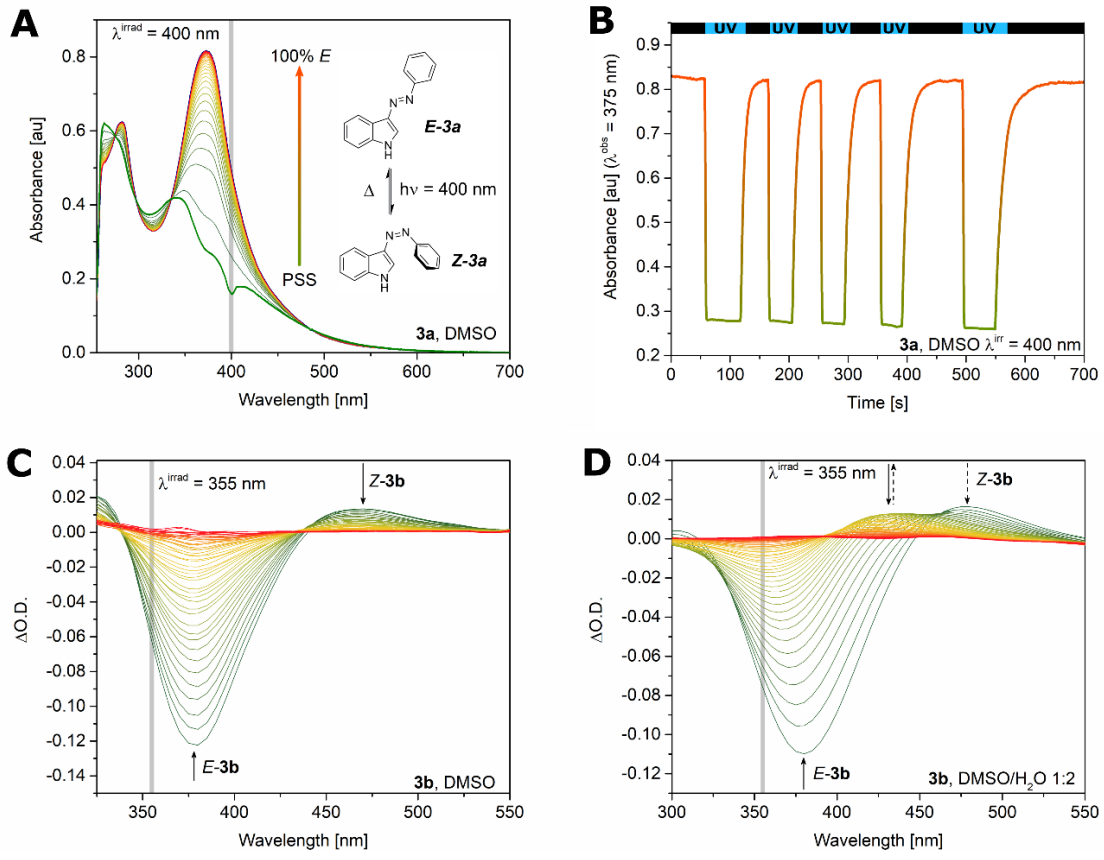

Figure 1. A: Thermal relaxation from the PSS (τ=4.3 s) of **3a** in DMSO after irradiation with λ^{irrad}=400 nm. **B**: Multiple isomerization cycles of **3a** in DMSO (black bars: dark, blue bars: irradiation with λ^{irrad}=400 nm; the observed wavelength corresponds to λ^{obs}=375 nm) indicating a good fatigue resistance. **C**: Transient signal registered for **3b** in DMSO. The disappearing of the n→π* band belonging to ***Z*-3b** is accompanied by the restoration of π →π* band of ***E*-3b**. **D**: Transient signal registered for **3b** in a

DMSO/water 1:2 mixture (detailed spectrometric data and kinetics in Section 3.3 in the Supporting Information). The decay of the n→π* band of ***Z*-3b** is followed by the formation of a hypsochromically shifted transient signal. Then, the π →π* band of ***E*-3b** reappears.

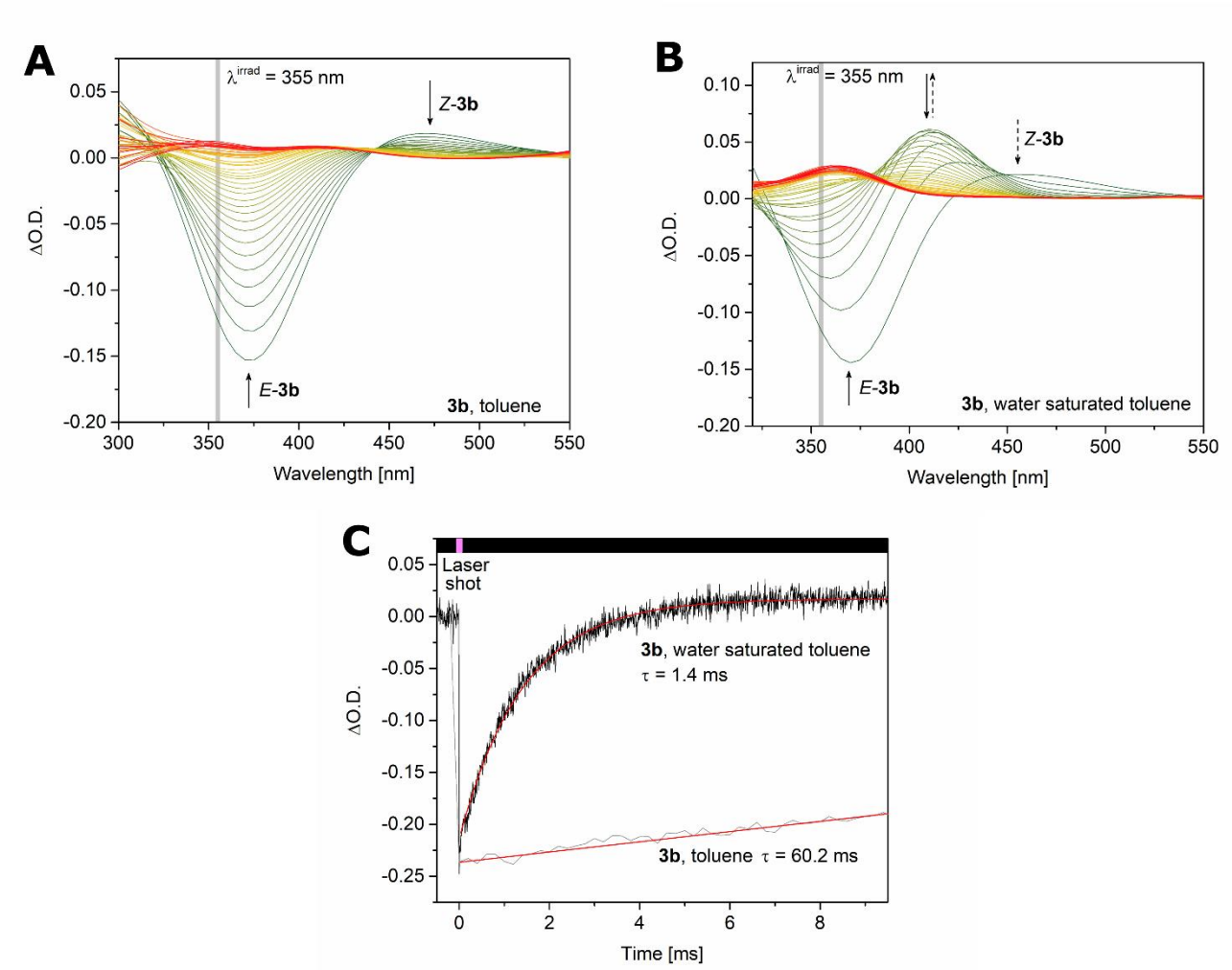

Figure 2. A: Thermal *Z*-*E* isomerization of compound **3b** in toluene. An isosbestic point can be observed, indicating the monomolecular decay of the n→π* band of ***Z*-3b** in favour of the formation of the π →π* of ***E*-3b**. **B**: The addition of water to toluene induces a change in the transient spectra. As like as in DMSO (cf. Figure 2d), a new species, blue-shifted compared to the n→π* band of ***Z*-3b**, can be detected by laser flash photolysis. This intermediate contributes to the restoration of the π →π* band of ***E*-3b**. **C**: Transient signal of the restoration of the π →π* band of ***E*-3b** (λ^{obs} =370 nm) in toluene and water saturated toluene. A forced protic environment inside toluene increases the overall *Z*-to-*E* isomerization rate.

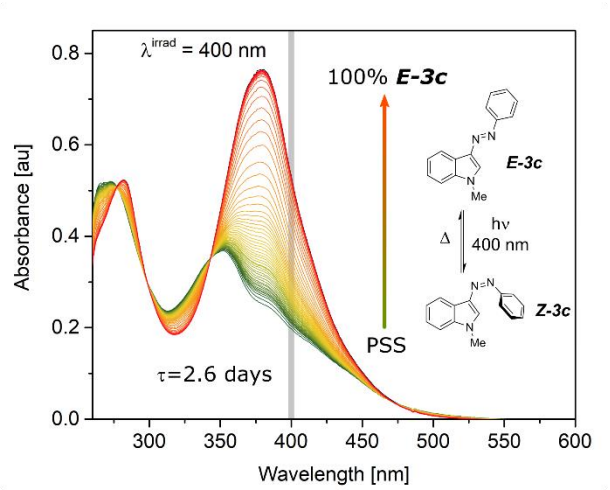

Figure 3. Thermal relaxation from the PSS (85:15 *Z*:*E* ratio, τ=2.6 d) of **3c** in DMSO after irradiation with λ^{irrad} = 400 nm.

The water content dependency led to an interesting saturation kinetic, that is another evidence of a mechanism characterized by an intermolecular proton transfer that is mediated by the presence of protic medium.

Moreover, we observed notable differences in the transient spectra of **3a**,**b**. In the absence of protic media, the transient signal of the *Z*-isomer directly interconverts to the *E*-form (that exhibits an isosbestic point in **3b**, where the n→π* absorption band of the *Z* form can be clearly discerned, see Figure 1C). However, in protic environment, the signal of ***Z*-3b** shifts hypsochromically, giving rise to a second band, which belongs to an intermediate of the *Z*-to-*E* thermal conversion that eventually collapses with the

restoration of the *E*-isomer (cf. Figure 1D). In **3a** a new band arises at a similar wavelength of the comparable one in **3b**, before the ***E*-3a** π→π* is restored). To prove our theory and to generalize the effect of a protic medium on the isomerization reaction of **3a,b**, we saturated toluene with water (cf. Figure 2 and Table 1, entry 6 for **3b**). Consequently, the isomerization rate increased sixtyfold and a transient signal, similar to the intermediate signal observed above, appears. Furthermore, the importance of the NH moiety in the thermal *Z*-to-*E* relaxation was proven studying compound **3c**. Indeed, the methylation of the indole-nitrogen (in **3c**) causes significant changes of the relaxation properties with respect to the N–H containing derivatives (**3a**,**b**). Compound **3c** exhibits longer lifetimes (minutes to days, see Table 1) compared to **3a**,**b**. Moreover, in polar-aprotic solvents (DMSO and MeCN) as well as in mesitylene, **3c** shows τ larger than one day. Owing to their stable photostationary state, we were able to determine the PSS population of **3c** in DMSO (Figure 3) and MeCN applying ^{1}H-NMR-spectroscopy (85:15 and 61:39 of *Z*:*E* ratio, respectively; see Section 4.4 in the Supporting Information).

However, to the best of our knowledge, spectroscopic observations similar to the ones we witnessed have not been made so far. Phenylazoindoles themselves are known to give rise to a hydrazone tautomerism.[36] Thus, we aimed to explain the involvement of an azo-hydrazone and why minimal modifications of the indolic core lead to a surprisingly wide span of thermal relaxation rates through a detailed computational study.

Computational studies. To seek for similarities with the azobenzene core, we endeavoured to analyze both the photochemical *E*-to-*Z* and thermal *Z*-to-*E* interconversion pathways. Representing the most general scaffold, **3a** was selected for the study. Hence, we performed an MS-CASPT2/CASSCF calculation of the *E*-to-*Z* pathway, both from the first (S1, n→π* in character; cf. Figure 4A) and the second excited state (S_2, π→π*). The analysis of the molecular structure, its electronic distribution and the *g* and *h* vectors defining the branching space of the conical intersections (CoIns) (cf. Figure 4A and B), helped us to assign the photochemical decay pathways (a complete analysis of the CoIns is present in Section 5.2.2 in the Supporting Information).[37] Similarly to azobenzene, population of the n→π* singlet excited state leads to a rotational conical intersection (S_0←S_1, $CoIn_A$), which generates the *Z*-isomer.[14] This process is barrierless. Excitation to the S_2 level is followed by a deactivation to S_1 via a conical intersection topologically similar to the S_0←S_1 one ($CoIn_C$). The molecule has now enough potential energy either to go through $CoIn_A$ relaxing to ***Z*-3a** or to funnel through another conical intersection to the sole ***E*-3a** isomer ($CoIn_B$). $CoIn_B$ is only accessible in this way, because it is located energetically uphill compared to the Franck-Condon geometry of the S_1.

In accordance with our experiments, the simulated photochemical behaviour of **3a**, and in general of phenylazoindole cores, do not differ drastically compared to the parent azobenzene photoswitch.[14] In contrast, the thermal *Z*-to-*E* pathway was studied via broken symmetry (BS)-DFT taking into account three different mechanisms, *viz.* the inversion, the rotation (both of them typical of azobenzene)[38] and the intermolecular hydrazone-formation (with and without water assisting molecules). We found that the indole moiety lowers the rotational activation barrier with respect to the inversion in **3a**-**b** ($\Delta E^{\ddagger}$=20.3 and 30.7 kcal/mol for the rotation and inversion mechanism, respectively, at the ωB97XD/6-31G(d) level of theory; Figure 3C; comparable findings were recently reported on arylazoindazoles[33]), while N-Me indole (**3c**) increases it ($\Delta E^{\ddagger}$=33.8 and 30.7 kcal/mol for the rotation and inversion mechanism, respectively, at the ωB97XD/6-31G(d) level of theory). That could be an explanation for the higher lifetimes encountered in aprotic solvents for **3c** compared to **3a** and **3b**, where other pathways, apart monomolecular relaxation, were not detected. The computed thermochemical values we have in hand ($\Delta H^{\ddagger}$=14 kcal/mol at the (C-PCM)-B3LYP/6-31G(d) in MeCN) are comparable with the experimental Eyring-Polanyi plot obtained for **3a** in MeCN ($\Delta H^{\ddagger}$=12 kcal/mol; Figure 4D)

Most interestingly, using DFT calculations we proved the participation of a hydrazone intermediate in a third relaxation pathway. We reasoned that the hydrazone formation in azoindoles is only feasible intermolecularly, due to the impossibility for the indolic proton to reach the azo group intramolecularly (see Scheme 2; Section 5.4 in the Supporting Information; for a more detailed representation of the mechanism see Section 8 of the Supporting Information).

Scheme 2. Simplified Intermolecular Hydrazone Mechanism

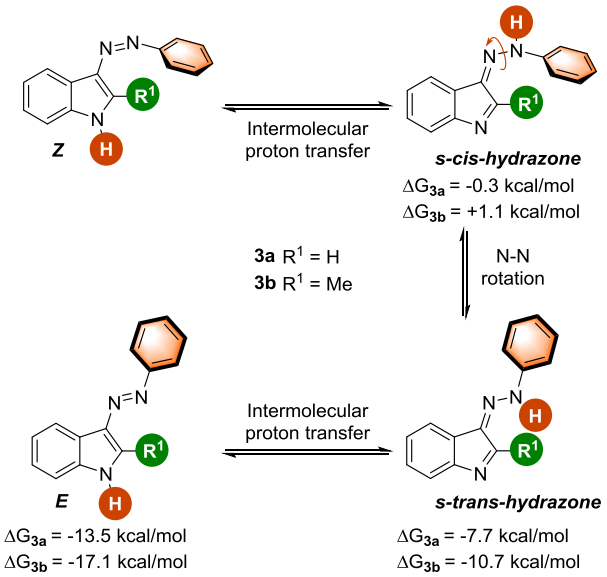

Level of theory: CPCM(DMSO)-B3LYP/6-31G(d)
Energies of the species compared to the *Z*-isomer, taken as a reference.

However, without the assistance of water (representing the simplest proton donor) the interaction of two molecules of **3a** is characterized by high energy barriers, which make this pathway not competitive with the previously analyzed monomolecular thermal isomerizations. On the other hand, two explicit molecules of water bridging two *Z*-conformers of **3a** lower the energetical barriers for the hydrazone formation, thus explaining the increase of rate observed with protic solvents in N-H containing azoindoles (Section 7 in the Supporting Information). We propose the

following mechanism. The first step involves a water-mediated proton transfer from the indole nitrogen of one molecule of ***Z*-3a** onto the azo-moiety of the second one (β-nitrogen atom with respect to the indole, see Figure 4C). The barrier for the formation of this complex is only 17.3 kcal/mol due to the stabilizing action of the water molecules. The ensuing generation of the two *s*-cis hydrazones is defined by a low activation energy ($\Delta E^{\ddagger}$=3.5 kcal/mol) and results to be slightly exothermal (ca. 1 kcal/mol). After the rotation around the newly formed N-N-single bonds (characterized by ($\Delta E^{\ddagger}$= 8.6 and 10.2 kcal/mol), the *s*-trans hydrazone dimer is formed, which is located inside a potential well (ca. 30 kcal/mol more stable than the initial water-bridged ***Z*-3a** dimer; see figure 4C). Due to this fact, the transient signal of the intermediate present in protic media can be assigned to the *s*-trans hydrazone (compare Figure 4E, showing the simulated TD-DFT UV/Vis spectra of the azohydrazone of **3b** with the experimentally observed band, figure 2D).

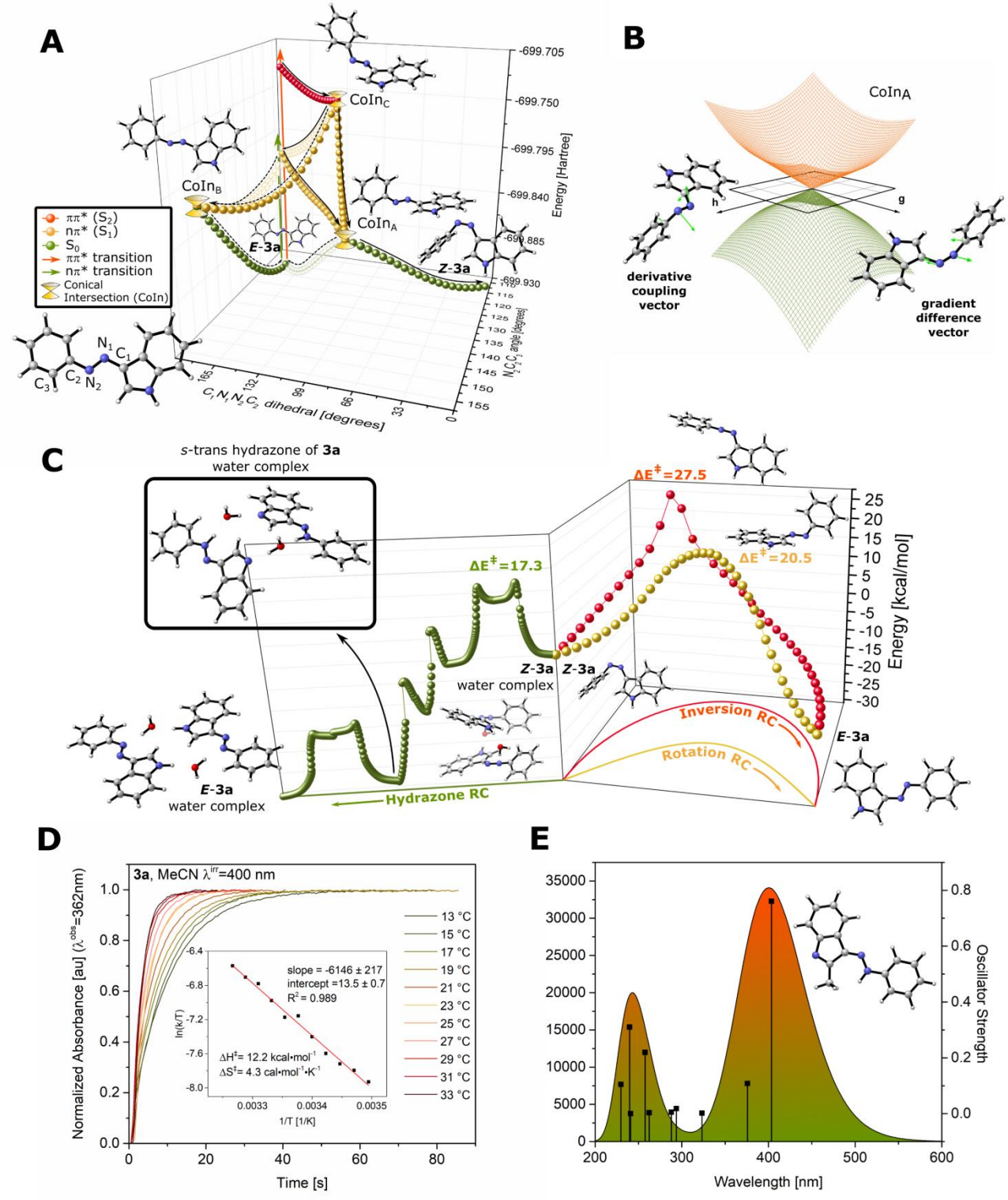

Figure 4. A: Photochemical *E*-to-*Z* isomerization pathways calculated at the CASSCF(10,8)/6-31G(d) level of theory, showing the different pathways **3a** can cover after excitation to the first or second excited state. **B:** Branching space of Conical Intersection A ($CoIn_A$) represented in figure A. The derivative coupling (*g*) and gradient difference vectors (*h*), removing the degeneracy between the S1 and S0, are highlighted with green arrows on the geometry at which the conical intersection occurs. **C:** Thermal reaction coordinates (RC) restoring ***E*-3a** from ***Z*-3a**. In particular, the rotation, inversion and hydrazone formation mechanisms are compared. In the box, the spectroscopically detectable hydrazone of **3a** is represented. **D:** Thermal relaxation kinetics of **3a** in MeCN at different temperatures. The related Eyring-Polanyi plot is depicted in the inset **E: (**TD)-PBE0/6-311+G(2d,p) simulated UV/Vis spectrum of the s-trans conformer of the azo-hydrazone of **3b** in DMSO. In the inset, the optimized structure of the same species is shown.

Then, the system undergoes two consecutive water-mediated proton-transfers leading to the *E*-isomer of **3a**. The hydrazone pathway possesses a slightly lower activation energy in protic media than the rotation or the inversion ones. This explains the surprisingly fast isomerization kinetics found with increased proton availability of the medium for **3a**,**b**.With this mechanism in hand, we also expect **3a** and **3b** to be able to switch faster at higher concentrations, nicely explaining the concentration-dependent behavior we found in our experiments (entry 11, Table 1; Section 7 in Supporting Information).

Moreover, the competition between the hydrazone and the rotation pathway can be recognized for **3b** in MeOH for its biexponential decay. In contrast, due to its methylated nitrogen atom, the azo-hydrazone formation is precluded to **3c**.

CONCLUSIONS

In summary, the photochromic properties of phenylazoindoles have been investigated for the first time. We synthesized compounds **3a-c** representing three very basic derivatives of this class of azo dyes. All compounds photoisomerize applying light of 355, 365 and 400 nm wavelength. Thereby, *N*-methylated **3c** showed the typical behaviour of an azobenzene (τ between several minutes to two days). In contrast to this findings, *N*-H azoindoles exhibit shorter lifetimes, strongly dependent on the protic character of the solvent. We took further advantage of this relationship and tuned the reaction kinetics, increasing the proton content of the solvents. Best results were obtained in mixtures of DMSO and water (1:1) using DBU as an additive, giving rise to lifetimes between 33.9 and 46 ns for **3a** or **3b**, respectively. The surprisingly short lifetimes are explained by a thorough mechanistic study, assuming the intermolecular formation of a hydrazone. Such a mechanism was studied in detail for the first time, spectroscopically, kinetically and computationally. Compared to the canonical inversion and rotation pathways, this conversion is energetically favoured in protic media. Thus, faster *Z*-to-*E* relaxation rates can be achieved for **3a**,**b** in contrast to **3c**. Hence, only slight changes of the substituent position or the solvent composition can drastically tune the properties of phenylazoindoles. Such extremely versatile properties render this core structure a suitable candidate for the wide range of applications of photoswitches.

ASSOCIATED CONTENT

Supporting Information. General procedures, synthesis of compounds **3a-c**, spectroscopic experiments, NMR experiments, computational analysis. This material is available free of charge via the Internet at http://pubs.acs.org.

AUTHOR INFORMATION

Corresponding Author

* E-mail: burkhard.koenig@chemie.uni-regensburg.de

ORCID

Nadja A. Simeth: 0000-0001-8130-883X
Stefano Crespi: 0000-0002-0279-4903
Maurizio Fagnoni: 0000-0003-0247-7585
Burkhard König: 0000-0002-6131-4850

Author Contributions

‡These authors contributed equally.

ACKNOWLEDGMENT

We are grateful to Regina Hoheisel and Julia Zach for technical support and to Prof. S. M. Bonesi (University of Buenos Aires) for his help with the kinetic analysis. This work was supported by CINECA SCAI, with computer time granted by ISCRA projects (project code: HP10CBEIAU and HP10C8U1NY). N.A.S. thanks the Studienstiftung des Deutschen Volkes for a doctoral scholarship. S.C. gratefully thanks P. Sbazzeguti, Prof. S. Protti and Dr. D. Ravelli for their help and fruitful discussions.

REFERENCES

(1) *Molecular Switches*; Feringa, B. L., Browne, W. R., Eds.; Wiley-VCH Verlag GmbH & Co. KGaA: Weinheim, Germany, 2011.

(2) Velema, W. A.; Szymanski, W.; Feringa, B. L. *J. Am. Chem. Soc.* **2014**, *136*, 2178–2191.

(3) Withers, N. *Nat. Chem.* **2010**, *2*, 11–11.

(4) Gelebart, A. H.; Jan Mulder, D.; Varga, M.; Konya, A.; Vantomme, G.; Meijer, E. W.; Selinger, R. L. B.; Broer, D. J. *Nature* **2017**, *546*, 632–636.

(5) Camacho-Lopez, M.; Finkelmann, H.; Palffy-Muhoray, P.; Shelley, M. *Nat. Mater.* **2004**, *3*, 307–310.

(6) del Valle, M.; Gutiérrez, R.; Tejedor, C.; Cuniberti, G. *Nat. Nanotechnol.* **2007**, *2*, 176–179.

(7) Baroncini, M.; d'Agostino, S.; Bergamini, G.; Ceroni, P.; Comotti, A.; Sozzani, P.; Bassanetti, I.; Grepioni, F.; Hernandez, T. M.; Silvi, S.; Venturi, M.; Credi, A. *Nat. Chem.* **2015**, *7*, 634–640.

(8) Banghart, M.; Borges, K.; Isacoff, E.; Trauner, D.; Kramer, R. H. *Nat. Neurosci.* **2004**, *7*, 1381–1386.

(9) Gautier, A.; Gauron, C.; Volovitch, M.; Bensimon, D.; Jullien, L.; Vriz, S. *Nat. Chem. Biol.* **2014**, *10*, 533–541.

(10) Vomasta, D.; Högner, C.; Branda, N. R.; König, B. *Angew. Chem. Int. Ed.* **2008**, *47*, 7644–7647.

(11) Simeth, N. A.; Kneuttinger, A. C.; Sterner, R.; König, B. *Chem Sci* **2017**, *8*, 6474–6483.

(12) Neilson, B. M.; Bielawski, C. W. *ACS Catal.* **2013**, *3*, 1874–1885.

(13) *Photochromism: molecules and systems*, Rev. ed.; Dürr, H., Bouas-Laurent, H., Eds.; Elsevier: Amsterdam ; Boston, 2003.

(14) Conti, I.; Garavelli, M.; Orlandi, G. *J. Am. Chem. Soc.* **2008**, *130*, 5216–5230.

(15) Bandara, H. M. D.; Burdette, S. C. *Chem Soc Rev* **2012**, *41*, 1809–1825.

(16) Andréasson, J.; Pischel, U.; Straight, S. D.; Moore, T. A.; Moore, A. L.; Gust, D. *J. Am. Chem. Soc.* **2011**, *133*, 11641–11648.

(17) García-Amorós, J.; Velasco, D. *Beilstein J. Org. Chem.* **2012**, *8*, 1003–1017.

(18) Kienzler, M. A.; Reiner, A.; Trautman, E.; Yoo, S.; Trauner, D.; Isacoff, E. Y. *J. Am. Chem. Soc.* **2013**, *135*, 17683–17686.

(19) Bléger, D.; Schwarz, J.; Brouwer, A. M.; Hecht, S. *J. Am. Chem. Soc.* **2012**, *134*, 20597–20600.

(20) Samanta, S.; McCormick, T. M.; Schmidt, S. K.; Seferos, D. S.; Woolley, G. A. *Chem. Commun.* **2013**, *49*, 10314.

(21) Garcia-Amorós, J.; Díaz-Lobo, M.; Nonell, S.; Velasco, D. *Angew. Chem. Int. Ed.* **2012**, *51*, 12820–12823.

(22) Venkataramani, S.; Jana, U.; Dommaschk, M.; Sonnichsen, F. D.; Tuczek, F.; Herges, R. *Science* **2011**, *331*, 445–448.

(23) Suwa, K.; Otsuki, J.; Goto, K. *Tetrahedron Lett.* **2009**, *50*, 2106–2108.

(24) Calbo, J.; Weston, C. E.; White, A. J. P.; Rzepa, H. S.; Contreras-García, J.; Fuchter, M. J. *J. Am. Chem. Soc.* **2017**, *139*, 1261–1274.
(25) Zhao, L.; Liu, J.; Zhou, P. *J. Phys. Chem. A* **2017**, *121*, 141–150.
(26) Otsuki, J.; Suwa, K.; Sarker, K. K.; Sinha, C. *J. Phys. Chem. A* **2007**, *111*, 1403–1409.
(27) Heitmann, G.; Schütt, C.; Herges, R. *Eur. J. Org. Chem.* **2016**, *2016*, 3817–3823.
(28) Weston, C. E.; Richardson, R. D.; Fuchter, M. J. *Chem Commun* **2016**, *52*, 4521–4524.
(29) Wendler, T.; Schütt, C.; Näther, C.; Herges, R. *J. Org. Chem.* **2012**, *77*, 3284–3287.
(30) Wang, Y.-T.; Liu, X.-Y.; Cui, G.; Fang, W.-H.; Thiel, W. *Angew. Chem. Int. Ed.* **2016**, *55*, 14009–14013.
(31) Stricker, L.; Fritz, E.-C.; Peterlechner, M.; Doltsinis, N. L.; Ravoo, B. J. *J. Am. Chem. Soc.* **2016**, *138*, 4547–4554.
(32) Weston, C. E.; Richardson, R. D.; Haycock, P. R.; White, A. J. P.; Fuchter, M. J. *J. Am. Chem. Soc.* **2014**, *136*, 11878–11881.
(33) Travieso-Puente, R.; Budzak, S.; Chen, J.; Stacko, P.; Jastrzebski, J. T. B. H.; Jacquemin, D.; Otten, E. *J. Am. Chem. Soc.* **2017**, *139*, 3328–3331.
(34) Barden, T. C. In *Heterocyclic Scaffolds II*; Gribble, G. W., Ed.; Springer Berlin Heidelberg: Berlin, Heidelberg, 2010; Vol. 26, pp 31–46.
(35) Ding, H.; Peng, Z.; Wang, J.; Lu, P.; Wang, Y. *Org Biomol Chem* **2016**, *14*, 7114–7118.
(36) Babür, B.; Seferoğlu, N.; Aktan, E.; Hökelek, T.; Şahin, E.; Seferoğlu, Z. *J. Mol. Struct.* **2015**, *1081*, 175–181.
(37) Olivucci, M.; Bernardi, F.; Celani, P.; Ragazos, I.; Robb, M. A. *J. Am. Chem. Soc.* **1994**, *116*, 1077–1085.
(38) Yu, L.; Xu, C.; Zhu, C. *Phys Chem Chem Phys* **2015**, *17*, 17646–17660.

Insert Table of Contents artwork here